J Multidisciplinary Scientific Journal

MDPI

Article

Comparative Screening of Ethyl Cellulose Grade, Casting Solvent, Plasticizer, and Nanofiller Effects on Solvent-Cast Film Properties

Elodie Melro *, Andreia S. R. Oliveira, Diana Farinha, Andreia A. S. Alves and Filipe E. Antunes *

Science 351–Disruptive & Sustainable R&D Innovations, HIESE, 3230-343 Coimbra, Portugal; andreia.oliveira@science351.pt (A.S.R.O.); diana.farinha@science351.pt (D.F.); andreia.alves@science351.pt (A.A.S.A.)

* Correspondence: elodie.melro@science351.pt (E.M.); filipe.antunes@science351.pt (F.E.A.)

Abstract

Conventional flexible food packaging often relies on multilayer structures based on non-biodegradable petrochemical materials to achieve the required barrier performance, generating persistent waste and making recycling difficult. Replacing these systems with simpler cellulose-derived alternatives remains challenging, particularly because moisture protection is difficult to achieve with inherently hygroscopic materials. Ethyl cellulose (EC) is a rare cellulose derivative that is hydrophobic, thermoplastic and, being an ether rather than an ester, hydrolytically stable. Yet much of the foundational knowledge of EC film formation comes from pharmaceutical coating, where permeability is deliberately engineered rather than suppressed, and where each study varies one parameter in its own matrix. However, their relative effects have rarely been compared using the same film-preparation and testing conditions. We prepared different EC film formulations at a fixed EC concentration of 5 wt.% and systematically varied commercial grade, solvent system, plasticizer, or nanofiller while maintaining consistent casting and testing conditions. Solvent system and plasticizer formulation produced significant differences in water vapor transmission rate (WVTR), whereas commercial EC grade and nanofiller type and loading did not significantly affect WVTR. Plasticizer formulation produced the widest variation in mechanical properties, with tensile strength ranging from 4 to 49 MPa, compared with 12–34 MPa across the solvent systems. Apparent M_n^{SEC} showed no consistent relationship with film performance; notably, the highest-M_n^{SEC} grade exhibited the lowest tensile strength among the seven commercial grades. Tributyl citrate and glycerol at 0.1 wt.% jointly gave the best strength–elongation balance; ZnO- and SiO_2-filled films showed the highest mean mechanical values but none differed significantly from the unfilled control.

Keywords: ethyl cellulose; solvent casting; plasticizers; nanofillers; water vapor transmission; packaging materials

Check for updates

Academic Editor: Javier Narciso

Received: 12 August 2026
Revised: 9 October 2026
Accepted: 19 October 2026
Published: 22 October 2026

Copyright: © 2026 by the authors. Licensee MDPI, Basel, Switzerland. This article is an open access article distributed under the terms and conditions of the Creative Commons Attribution (CC BY) license.

1. Introduction

Ethyl cellulose (EC) is a cellulose derivative obtained by partial substitution of hydroxyl groups of cellulose with ethoxyl groups [1]. Commercial EC grades typically contain 46.5–49.5% ethoxyl groups, corresponding to a degree of substitution (DS) of approximately 2.4–2.6 [2]. Ethyl cellulose is a semisynthetic cellulose-derived polymer that is generally regarded as non-toxic, odorless, colorless, and biocompatible. At this degree of substitution, EC is insoluble in water but soluble in several organic solvents and solvent mixtures due to

the coexistence of residual hydroxyl groups and hydrophobic ethoxyl substituents along the polymer backbone.

Ethyl cellulose films intended for packaging applications are commonly prepared by solvent casting at laboratory scale, in which a polymer solution is cast onto a support and subjected to controlled solvent evaporation, forming the polymeric film. EC films are generally described by manufacturers as mechanically tough, thermoplastic and flexible, remaining flexible at temperatures as low as −40 °C even when unplasticized, which distinguishes them from other, more brittle cellulose esters and ethers [1]. However, the properties of EC are governed by the solvent used, since it determines the degree of chain extension in solution, the evaporation kinetics and the resulting film morphology. Arwidsson and Nicklasson identified methylene chloride:ethanol (60:40, *w*/*w*) as a suitable solvent system for dissolving EC [3], while the system toluene:ethanol (80:20, *w*/*w*) is widely used as the industrial reference for viscosity grading. Azoury et al. demonstrated that EC films cast from ethanol exhibit a greater capacity for water binding and form a thicker hydration layer than films prepared from chloroform, highlighting the influence of the casting solvent on moisture-barrier performance [4]. More recently, Horvat et al. reported that EC films produced using ethyl lactate showed lower oxygen and water vapor permeability, as well as high contact angles, compared with films cast from ethanol [5].

Polymer molecular weight can influence chain entanglement, molecular mobility, and the mechanical behavior of polymer films. In commercial EC, however, viscosity grade and molecular weight may also be accompanied by differences in degree of substitution, substitution pattern, molecular weight distribution, and manufacturing history. Consequently, comparisons between commercial grades should be interpreted as reflecting the combined effects of molecular weight and other grade-specific characteristics. Davidovich-Pinhas et al. verified that the glass transition temperature of EC (in powder form) increased with molecular weight [6]. In this study they also reported a semicrystalline morphology characterized by nanoscale crystalline domains.

Unplasticized EC films may exhibit relatively high stiffness and limited elongation. Plasticizers are therefore commonly incorporated to increase chain mobility and reduce brittleness. Compounds previously evaluated in EC films include castor oil [7], triethyl citrate, triacetin, diethyl phthalate [8], and dibutyl sebacate [9]. Depending on plasticizer type, concentration, and compatibility with EC, their incorporation generally decreases tensile strength and modulus and may increase elongation at break.

Nanofillers have also been investigated as a strategy to modify the mechanical, barrier, surface, and functional properties of EC films. Cellulose nanocrystals have been reported to reinforce EC matrices under suitable dispersion and interfacial conditions [10]. Modified nanocellulose may also improve mechanical and oxygen-barrier properties, although its effectiveness depends strongly on surface chemistry and compatibility with the comparatively hydrophobic EC matrix [11]. Inorganic nanofillers, including silica and metal oxide nanoparticles, may provide additional reinforcement or functional properties, but their effects depend on particle size, dispersion, concentration, and filler–matrix interactions.

Although EC grade, casting solvent, plasticizer selection, and nanofiller incorporation have individually been investigated in previous studies, comparative screenings covering these variables within a consistent film-preparation framework remain limited. The present work evaluates the effects of commercial EC grade, solvent system, plasticizer type and concentration, and nanofiller type and concentration on the barrier-related, surface, and mechanical properties of solvent-cast EC films. The different variables were screened sequentially using a nominal EC concentration of 5 wt.%, with the aim of identifying promising individual formulation conditions for subsequent combined optimization. Given the broad formulation space investigated, the present study was designed as a preliminary

screening to identify promising formulation conditions for subsequent optimization and independent batch validation.

2. Materials and Methods

2.1. Materials

Ethyl cellulose samples were purchased from Tokyo Chemical Industry Co. (TCI, Tokyo, Japan) and Thermo Scientific, while additional grades were kindly provided by IFF. The commercial grades used in this study, together with their abbreviations, viscosity ranges, and suppliers, are listed in Table 1.

Table 1. Commercial ethyl cellulose (EC) grades used in this study, including the assigned abbreviations, supplier-reported viscosity range (5% *w*/*w* in toluene/ethanol 80:20), and supplier.

Name	Abbreviation	Viscosity (mPa·s)	Supplier
Ethocel™ Standard 10	Ethocel 10	9–11	IFF
Ethyl cellulose	EC 18–22	18–22	TCI
Ethocel™ Standard 45	Ethocel 45	41–49	IFF
Ethyl cellulose	EC 45–55	45–55	TCI
Ethyl cellulose	EC 90–110	90–110	TCI
Ethocel™ Standard 200	Ethocel 200	180–220	IFF
Ethyl cellulose	EC 300	300	Thermo Scientific

Ethanol (E, 96%), acetone (99.6%), isopropanol (IPA, 99.8%), and glycerol (99.97%) were obtained from José Manuel Gomes dos Santos (JMGS, Lisbon, Portugal). Acetic acid (AA, 99.7%) and ethyl acetate (99.8%) were purchased from Fisher Chemical (Waltham, MA, USA). Triacetin (>99.0%), tributyl citrate (>98.0%), dimethyl sebacate (>98.0%), dibutyl sebacate (>98.0%), and methyl oleate (>60.0%) were supplied by TCI Chemicals. Sorbitol (>97%) was obtained from Camassia (Almería, Spain). Cellulose nanocrystals (CNC, >96%), cellulose nanofibrils (CNF, >99%), silica nanoparticles (SiO_2, ≥99.5%), and zinc oxide nanoparticles (ZnO, 99.5%) were purchased from Nanografi (Ankara, Turkey). Supplier-reported technical specifications of the commercial nanofillers, including nominal dimensions, morphology, specific surface area, crystallinity and density, are summarized in Table S1.

2.2. Methods

2.2.1. Number-Average Molecular Weight of EC

As the technical data sheets of the seven commercial EC grades reported only nominal viscosity ranges (5% *w*/*w* in toluene:ethanol 80:20) and not molecular weight, this parameter was determined by high-performance size-exclusion chromatography (HPSEC; Viscotek TDAmax, Malvern, UK), equipped with a differential viscometer, right-angle laser-light scattering, low-angle laser-light scattering, and refractive index detectors. The column set consisted of a PL guard column (50 × 7.5 mm), followed by a Viscotek T200 column (6 µm), a Viscotek T3000 column (6 µm), and a Viscotek LT4000L column (7 µm). An HPLC dual-piston pump delivered the eluent, tetrahydrofuran, previously filtered through a 0.2 µm filter, at a flow rate of 1 mL/min. The system was equipped with an on-line degasser, and analyses were performed at 30 °C. Prior to injection (100 µL), samples were filtered through a polytetrafluoroethylene membrane with 0.2 µm pore size. The SEC system was calibrated using 7 narrow-molecular-weight-distribution polystyrene standards covering a molecular-weight range of 1820 to 201,000 g/mol, and molecular weight distributions were determined by conventional SEC calibration. Therefore, the molecular weight (M_n^{SEC}) values reported in this study correspond to apparent molecular weights relative to polystyrene standards. All EC grades exhibited dispersity values

(Đ = Mw/Mn) above 1.5. Each EC grade was analyzed once; therefore, analytical repeatability and measurement uncertainty were not assessed. Data were processed using OmniSEC software, version 4.6.1.354.

2.2.2. EC Film Preparation

In all experiments, EC was incorporated at a concentration of 5 wt.%, calculated relative to the total mass of the final film-forming solution. A mass of 20 g of each film-forming solution was cast into polystyrene/polytetrafluoroethylene Petri dishes with an internal diameter of 90 mm and dried at 50 °C, in a forced-air oven, for approximately 16 h to obtain free-standing films. The specific preparation procedure used for each experimental series is described below.

To evaluate the effect of commercial EC grade, each of the seven EC grades listed in Table 1 was incorporated at 5 wt.% in E:W (90:10, v/v). The formulations were stirred magnetically for 24 h at room temperature to promote complete polymer dissolution. Ethocel™ Standard 45 (IFF, New York, NY, USA) was selected as a representative intermediate-viscosity grade for the subsequent solvent, plasticizer, and nanofiller screenings. To investigate the effect of solvent composition, Ethocel™ Standard 45 was incorporated at 5 wt.% in acetone, ethyl acetate, AA, IPA, E, E:W (90:10, v/v), E:AA (90:10, 80:20, and 70:30, v/v), and IPA:AA (80:20, v/v). The formulations were stirred magnetically for 24 h at room temperature.

For the plasticizer screening, glycerol, sorbitol, triacetin, tributyl citrate, dimethyl sebacate, dibutyl sebacate, and methyl oleate were individually incorporated into EC formulations prepared in E:W (90:10, v/v). Plasticizer concentrations of 0.1 and 1 wt.% were calculated relative to the total mass of the final film-forming solution. Since the EC concentration was fixed at 5 wt.%, these concentrations corresponded to plasticizer loadings of 2 and 20 wt.% relative to the mass of EC, respectively. EC and the respective plasticizer were dissolved simultaneously under magnetic stirring for 24 h at room temperature before casting. The reported plasticizer concentrations correspond to the nominal amounts added to the film-forming solutions; the actual plasticizer content retained in the dried films after 16 h at 50 °C was not determined.

For the nanofiller screening, EC was first incorporated at 5 wt.% in E:W (90:10, v/v) and stirred magnetically for 24 h at room temperature to promote polymer dissolution. CNC, CNF, SiO_2 and ZnO were then individually dispersed in the previously prepared EC solutions at concentrations of 0.1 and 0.5 wt.% relative to the total mass of the final film-forming dispersion. These concentrations corresponded to filler-to-EC mass ratios of 2 and 10 wt.%, respectively. After nanofiller addition, the dispersions were mixed by magnetic stirring at 500 rpm for 30 min before casting. Magnetic stirring was selected as a simple and standardized dispersion method for the comparative nanofiller screening, allowing all fillers to be processed under the same conditions. Because the nanofillers remained as a dispersed solid phase, the resulting materials are hereafter referred to as EC nanocomposite films. To facilitate comparison among fillers with different densities, the filler volume fraction in the dried EC/filler composite was estimated according to $\varphi f = (mf/\rho f)/[(mf/\rho f) + (mEC/\rho EC)]$, where mf and mEC are the filler and EC masses and ρf and ρEC are their respective densities. Using a representative EC density of 1.14 g cm^{-3} and the supplier-reported filler densities, the 0.1 and 0.5 wt.% formulation loadings correspond approximately to 1.5 and 7.1 vol.% for CNC, 1.5 and 7.1 vol.% for CNF, 1.0 and 4.9 vol.% for SiO_2, and 0.4 and 2.0 vol.% for ZnO, respectively.

2.2.3. EC Film Characterization

Water vapor transmission rate (WVTR) was estimated through a gravimetric procedure adapted from the ASTM E96 water method [12]. Permeation cups were filled with distilled water and sealed with circular film specimens, exposing a defined film area of 4.15 cm^2. A headspace of 2 cm was maintained between the water surface and the film. The film surface that had been in contact with the Petri dish during casting was oriented toward the water inside the permeation cup. The cups were placed in a controlled chamber maintained at 32 °C and 50% relative humidity and weighed at time zero and after 24 h. WVTR was calculated from the mass loss of the cup over this interval, normalized to the exposed film area and time, and expressed in g/(m^2·day). Measurements were performed in triplicate.

Water absorption (WA) was determined based on ASTM D570 [13] and ISO 62 [14], adapted for square specimens (1 × 1 cm) cut from the films. Specimens were dried in an oven at 50 °C for 24 h, cooled in a desiccator, and weighed (W_0). Then they were immersed in distilled water for 24 h at room temperature in a closed system. After immersion, surface water was removed with absorbent paper, and the specimens were immediately reweighed (W_1). Water absorption (%) was calculated as $[(W_1 - W_0)/W_0] \times 100$. Measurements were performed in triplicate.

Water contact angle (WCA) was measured by the sessile drop method, using an automatic contact angle meter (Attension Theta Flex, Biolin Scientific, Gothenburg, Sweden). Film specimens were cut to a width of ca. 15 mm, following ASTM D5725 [15], to minimize curvature during testing. Distilled-water droplets (6 µL) were deposited on the air-facing surface of each film and images were acquired at 33 frames s^{-1} for 5 s. For each frame, the left and right contact angles were determined and averaged. The value assigned to each droplet and used in the main comparative analysis was the temporal mean of the averaged left–right contact angles recorded over the complete 5 s acquisition period. Three droplets were measured per formulation. To assess short-time wetting/spreading, WCA was additionally extracted immediately after complete droplet deposition (t = 0 s) and after 1 and 5 s, and the change in contact angle was calculated as $\Delta WCA = WCA_{5s} - WCA_{0s}$. The influence of droplet volume was evaluated on two representative EC films using 2, 4 and 6 µL water droplets (n = 3 per volume).

Mechanical properties were determined using an Instron 5944 universal testing machine equipped with a 500 N load cell, following a procedure based on ASTM D882 [16]. Rectangular specimens measuring 70 × 10 mm were tested at a crosshead speed of 5 mm/min and an initial grip separation of 41 mm. The thickness of each of the three tensile specimens was measured immediately before testing using a digital micrometer (Dexter, marketed by Leroy Merlin, Lille, France; resolution: 0.01 mm), and the specimen-specific thickness was used to calculate tensile stress. Tensile strength, elongation at break, and Young's modulus were determined from the resulting stress–strain curves. For graphical presentation, one tensile stress–strain curve per formulation was selected to illustrate the mechanical response (Figures S1, S4, S6, and S9), while the quantitative tensile properties correspond to the mean ± standard deviation of three specimens.

Infrared spectra of the different films were recorded with a Thermo Nicolet 380 Fourier transform infrared (FT-IR) apparatus equipped with a Smart Orbit Diamond ATR system (Thermo Scientific, Waltham, MA, USA). The spectra were obtained in absorbance mode from 4000 to 400 cm^{-1}, with a total of 32 scans and a resolution of 2 cm^{-1}. The background spectrum was collected with air before analyzing each sample. For graphical presentation, the FTIR spectra were normalized using OriginPro software 2026b (OriginLab Corporation, Northampton, MA, USA) to facilitate comparison of spectral features between samples; no quantitative interpretation was based on normalized absorbance intensities.

Film surface morphology was examined by scanning electron microscopy (SEM) using a VEGA3 SBH from TESCAN (Brno, Czech Republic). The samples were deposited on the carbon tape on the support and sputtered with a ca. 6 nm thin Au/Pd film, by cathodic pulverization using an SPI Module Sputter Coated (SPI Supplies, West Chester, PA, USA), for 90 s at a current of 15 mA. The accelerating voltage used ranged from 5 to 15 kV, and the work distance was set to 10 mm.

2.2.4. Statistical Analysis

Results are expressed as mean ± standard deviation. For each formulation, one film was independently cast. For WVTR, WA, and tensile measurements, the three replicates corresponded to specimens obtained from different regions of the same cast film. For WCA measurements, $n = 3$ corresponded to three individual droplets measured on the same film. Thus, these measurements represent within-film technical replicates rather than independent film-production replicates. The statistical analysis therefore reflects variability within a given casting and does not assess film-to-film or batch-to-batch reproducibility. Statistical differences among formulations were assessed by one-way analysis of variance (ANOVA), followed by Tukey's honestly significant difference (HSD) post hoc test at a significance level of $p < 0.05$. The results should consequently be interpreted within the context of this preliminary screening study.

3. Results and Discussion

3.1. Relationship Between Commercial EC Grade, Apparent Molecular Weight, and Film Properties

Since the technical data sheets of the commercial EC samples evaluated in this study reported viscosity ranges rather than molecular weight values, the M_n^{SEC} of each sample was determined by SEC. A broad tendency toward higher apparent M_n^{SEC} with increasing supplier-reported viscosity grade was observed (Table 2); however, the relationship was not one-to-one. Viscosity grade should not be interpreted as a direct measure of molecular weight, since solution viscosity is influenced not only by molecular weight but also by molecular-weight distribution, chain conformation and architecture, degree and pattern of substitution, polymer–solvent interactions, concentration, and temperature. Previous studies using fractionated EC under controlled conditions have reported positive relationships between intrinsic viscosity and molecular weight, while also demonstrating that the quantitative relationship depends on the solvent system and molecular characteristics of the polymer [3]. Accordingly, commercial EC viscosity grade is more appropriately considered an indirect rheological classification rather than a direct molecular-weight measurement. This is illustrated by Ethocel™ Standard 45 and EC 45–55, which have overlapping supplier-reported viscosity ranges (41–49 and 45–55 mPa·s, respectively) but exhibited different apparent M_n^{SEC} values (47,000 and 33,000 g/mol, respectively). Since these commercial grades originate from different suppliers and may also differ in molecular-weight distribution, degree and pattern of substitution, and manufacturing history, this difference cannot be attributed to molecular weight alone.

To assess the influence of EC grade on film properties, films were prepared using the seven commercial EC grades listed in Table 1, covering a molecular weight range from 18,000 to 104,200 g/mol, while maintaining E:W (90:10, v/v) as a fixed casting solvent. As the evaluated grades originated from different suppliers, the observed effects should be interpreted as the combined influence of molecular weight and potential differences in other grade-specific characteristics, such as DS and MWD. WVTR did not differ significantly among the seven commercial EC grades, ranging between ca. 315 and 362 g/(m^2·day) with no discernible trend across the tested M_n range, Figure 1. Water absorption showed the same pattern, with no significant differences detected among grades (Figure 2). The absence

of a clear relationship between apparent M_n^{SEC} and transport properties is consistent with previous observations in EC–ethanol–water systems [17], where the study revealed that film porosity was primarily governed by solvent composition, while polymer concentration had only a minor effect and M_n an even smaller one. Although their study employed spray coating rather than solvent casting, the overall conclusion that M_n plays a secondary role relative to solvent composition is consistent with the present results. A contrasting trend has been reported in blended EC/hydroxypropyl cellulose (HPC) films, where permeability decreased with increasing EC molecular weight [18]; however, that system involves a second polymer and phase-separation behavior between EC and HPC that is not present in the single-polymer films examined here, so the two results are not directly comparable.

Table 2. Number-average molecular weight, M_n^{SEC}, of the commercial EC grades used in this study, determined by high-performance size-exclusion chromatography (HPSEC) relative to polystyrene calibration standards. All EC grades exhibited dispersity values (Đ = Mw/Mn) above 1.5.

Sample	Molecular Weight (g/mol)
Ethocel 10	18,000
EC 18–22	26,400
Ethocel 45	47,000
EC 45–55	33,000
EC 90–110	62,200
Ethocel 200	79,500
EC 300	104,200

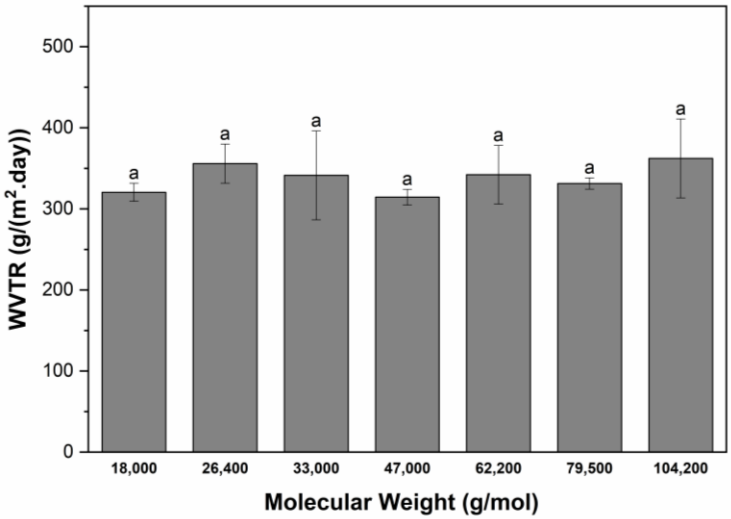


Figure 1. Water vapor transmission rate (WVTR) of ethyl cellulose (EC) films (5 wt.%, E:W 90:10) with different M_n. Results are presented as mean ± standard deviation (n = 3). Different letters above the bars indicate statistically significant differences between formulations according to one-way ANOVA followed by Tukey's HSD post hoc test ($p < 0.05$).

Using the temporal mean WCA recorded over the 5 s acquisition period (Figure 2), no significant differences were detected among the seven commercial EC grades. Mean WCA values ranged from 72° to 82°, and all grades belonged to the same Tukey group. Accordingly, surface wettability showed no statistically significant or monotonic relationship with apparent M_n^{SEC} over the range evaluated. This result further supports the conclusion that apparent molecular weight alone was not a reliable predictor of film performance across the commercial EC grades examined.

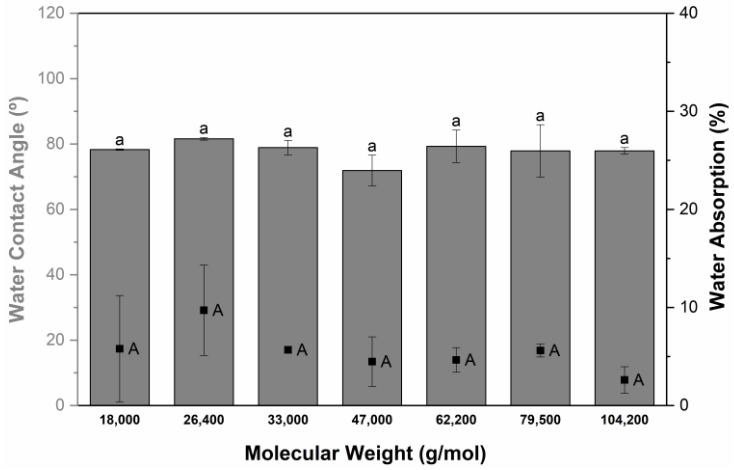


Figure 2. Water contact angle (bars, left axis) and water absorption (■, right axis) of EC films (5 wt.%) with different M_n. Results are expressed as mean ± standard deviation (n = 3). Different letters indicate statistically significant differences within each property according to one-way ANOVA followed by Tukey's HSD post hoc test ($p < 0.05$). Water contact angle and water absorption were analyzed independently.

Analysis of the mechanical properties showed that Young's modulus did not differ significantly among the seven commercial EC grades, ranging from ca. 1309 to 2151 MPa, Table 3. The absence of a clear relationship between Young's modulus and apparent M_n^{SEC} suggests that the small-strain elastic response of these films was not governed by molecular weight alone. Instead, it may reflect a similar balance of local chain packing and intermolecular interactions among the commercial grades, while any effect of molecular weight may have been masked by other grade-specific characteristics. Tensile strength and elongation at break, by contrast, varied significantly among commercial grades but did not show a monotonic relationship with apparent molecular weight. Only the 26,400 and 79,500 g/mol grades formed the significantly higher tensile-strength subgroup (46 and 48 MPa, respectively), while all other grades formed a significantly lower subgroup (18–28 MPa). Elongation at break followed a similar, even sharper pattern: only the 79,500 g/mol grade differed significantly from the rest (8.9%), while all remaining grades, including 26,400 g/mol despite its high tensile strength, formed a low-elongation subgroup (1.2–4.3%).

Table 3. Tensile strength, elongation at break, and Young's modulus of EC films (5 wt.%) with different M_n. Results are expressed as mean ± standard deviation (n = 3). Different lowercase superscript letters within the same column indicate statistically significant differences between formulations according to one-way ANOVA followed by Tukey's HSD post hoc test ($p < 0.05$).

Molecular Weight (g/mol)	Tensile Strength (MPa)	Elongation at Break (%)	Young's Modulus (MPa)
18,000	23.1 ± 6.7 ^{b}	1.7 ± 0.7 ^{b}	1594 ± 145 ^{a}
26,400	46.4 ± 7.0 ^{a}	4.3 ± 2.3 ^{b}	2151 ± 294 ^{a}
33,000	28.0 ± 2.3 ^{b}	2.5 ± 0.2 ^{b}	1478 ± 101 ^{a}
47,000	24.0 ± 5.2 ^{b}	2.1 ± 0.7 ^{b}	1484 ± 28 ^{a}
62,200	21.1 ± 7.2 ^{b}	1.2 ± 0.5 ^{b}	1892 ± 23 ^{a}
79,500	47.8 ± 11.0 ^{a}	8.9 ± 2.6 ^{a}	1888 ± 508 ^{a}
104,200	18.2 ± 1.9 ^{b}	1.6 ± 0.0 ^{b}	1309 ± 86 ^{a}

The tensile strength results do not follow the classical molecular weight–entanglement relationship, as the highest-M_n grade (104,200 g/mol) exhibited the lowest strength, while the strongest films were obtained at intermediate M_n values (26,400 and 79,500 g/mol).

These results indicate that M_n alone was not a reliable predictor of mechanical performance across the commercial grades evaluated. All EC samples exhibited relatively broad molecular-weight distributions, with dispersity values (Đ) above 1.5, and the grades originated from different manufacturers. Therefore, differences in molecular-weight distribution, degree and pattern of substitution, and manufacturing history may also have contributed to the observed mechanical behavior. These factors were not independently varied in the present screening, and their individual contributions cannot therefore be resolved. Previous studies have identified DS as a key parameter governing EC structure and mechanical behavior [19], while differences in MWD can alter strength and toughness independently of the M_n. Therefore, the present comparison should be interpreted as a screening of commercial EC grades rather than as an isolated evaluation of molecular-weight effects, since molecular weight was not varied independently from other grade-specific characteristics. Selected tensile stress–strain curves for the seven EC grades are provided in Figure S1 and illustrate the grade-dependent differences in tensile response summarized in Table 3.

3.2. Effect of Solvent Type on the Barrier, Surface, and Mechanical Properties of EC Films

The solvent system significantly affected WVTR, Figure 3. IPA produced the highest mean WVTR, ca. 461 g/(m^2·day), and was significantly different from most of the other systems. E:AA 80:20 produced the lowest mean WVTR, ca. 282 g/(m^2·day). However, it was not statistically different from pure acetic acid, acetone, ethanol, E:W 90:10, E:AA 90:10, or E:AA 70:30. Therefore, E:AA 80:20 should be described as the formulation with the lowest mean WVTR rather than as a statistically distinct optimum. The observed WVTR differences may be discussed in terms of the combined effects of solvent–polymer affinity and solvent evaporation kinetics. Hansen solubility parameters provide a useful framework for considering polymer–solvent compatibility, as the dispersion, polar, and hydrogen-bonding components jointly determine the distance between a solvent and a polymer in Hansen space [20]. Since EC-specific Hansen parameters and relative energy difference values were not determined for the solvent mixtures used here, specific mechanisms involving poor-solvent-induced vitrification or changes in free volume remain hypothetical. Acetic acid may interact with the residual hydroxyl and ether groups of EC and, due to its comparatively low volatility, may influence chain organization during drying. Thus, the low mean WVTR of E:AA 80:20 may be associated with differences in solvent affinity and film-formation history, although denser chain packing was not directly demonstrated [21].

The solvent system significantly affected the apparent WCA, Figure 4. Ethyl acetate produced the highest mean WCA (98.6 ± 4.7°) and was significantly higher than all other solvent systems. Pure acetic acid showed the second-highest mean value (85.6 ± 3.2°) and was significantly higher than E:W 90:10 (71.9 ± 4.7°), which presented the lowest mean WCA. The remaining solvent systems exhibited intermediate values and were not significantly different from either acetic acid or E:W 90:10. Importantly, E:AA 80:20 presented an intermediate WCA (80.5 ± 5.4°) despite producing the lowest mean WVTR. This confirms that short-time surface wettability and water-vapor transport through the complete film thickness are not directly coupled.

IPA produced the highest mean WA (ca. 6%) whereas ethanol produced the lowest mean value (ca. 3%). According to the Tukey groupings, IPA was significantly different from ethanol but not from the remaining solvent systems. These results indicate that surface wettability and bulk liquid-water uptake were not directly correlated under the tested conditions.

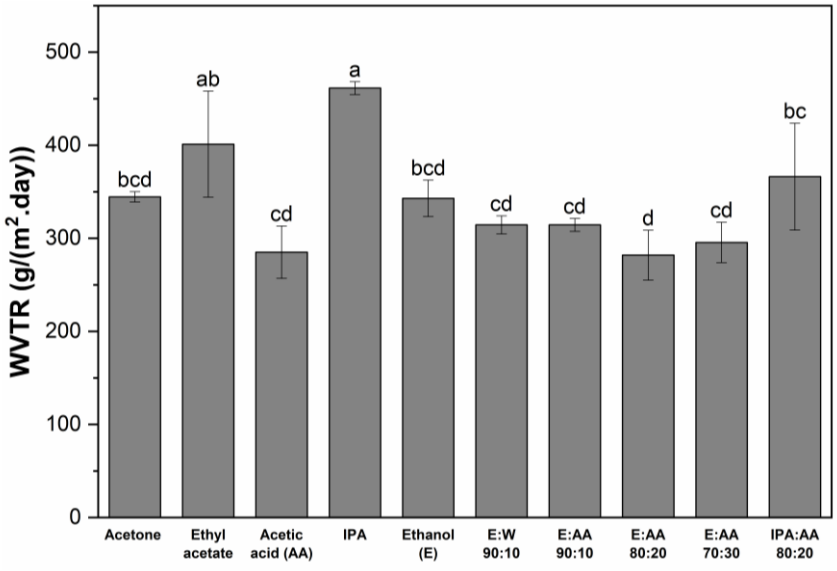


Figure 3. Water vapor transmission rate (WVTR) of EC films (5 wt.%, M_n 47,000 g/mol) prepared using different solvent systems. Results are presented as mean ± standard deviation (n = 3). Different letters above the bars indicate statistically significant differences between formulations according to one-way ANOVA followed by Tukey's HSD post hoc test ($p < 0.05$).

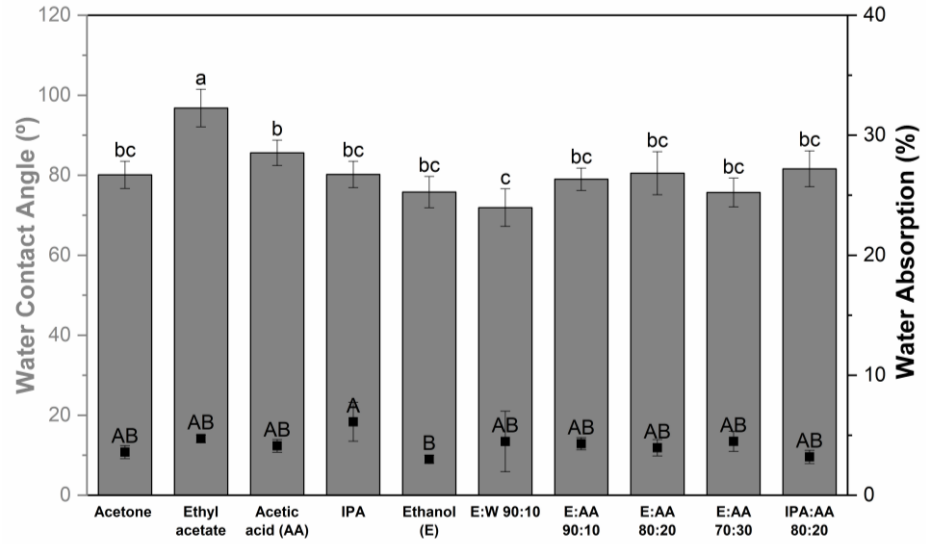


Figure 4. Water contact angle (bars, left axis) and water absorption (■, right axis) of EC films (5 wt.%, M_n 47,000 g/mol) prepared using different solvent systems. Results are expressed as mean ± standard deviation (n = 3). Different letters indicate statistically significant differences within each property according to one-way ANOVA followed by Tukey's HSD post hoc test ($p < 0.05$). Water contact angle and water absorption were analyzed independently.

The normalized ATR-FTIR spectra of films cast from E:W 90:10 and E:AA 80:20 were highly similar and retained the characteristic EC spectral fingerprint (Figure S3) [5]. No new prominent absorption bands or major spectral shifts were observed for the E:AA 80:20 film, indicating that the solvent-dependent differences in WVTR and mechanical behavior were not associated with formation of new covalent functionalities detectable by FTIR. The observed differences are therefore more consistent with physical effects arising during film formation, such as solvent–polymer interactions, evaporation history and chain organization. The normalized ATR-FTIR spectra do not, however, provide a quantitative assessment of residual acetic acid.

The solvent choice also influenced the mechanical properties of the films, Table 4. Acetone- and IPA-cast films presented the lowest mean tensile-strength values, approximately 12 MPa. Their tensile strength was significantly lower than that of several solvent systems, although it was not statistically different from that of E:W 90:10. These films also showed low mean elongation at break, but their values were statistically similar to those obtained with ethanol and, in some cases, E:W 90:10. The results therefore indicate comparatively weak and poorly extensible mechanical behavior under the tested conditions.

Table 4. Tensile strength, elongation at break, and Young's modulus of EC films (5 wt.%, M_n 47,000 g/mol) prepared with different solvent systems, with the three specimens obtained from different regions of the same cast film for each formulation. Results are expressed as mean ± standard deviation (n = 3). Different lowercase superscript letters within the same column indicate statistically significant differences between formulations according to one-way ANOVA followed by Tukey's HSD post hoc test ($p < 0.05$).

Solvent	Tensile Strength (MPa)	Elongation at Break (%)	Young's Modulus (MPa)
Acetone	11.8 ± 1.5 ^{b}	1.3 ± 0.1 ^{c}	1019 ± 64 ^{de}
Ethyl acetate	33.6 ± 6.0 ^{a}	8.9 ± 6.6 ^{ab}	1249 ± 28 ^{bcd}
Acetic acid (AA)	33.8 ± 1.4 ^{a}	10.0 ± 2.3 ^{a}	1449 ± 59 ^{abc}
IPA	11.9 ± 2.9 ^{b}	1.6 ± 0.5 ^{c}	878 ± 121 ^{e}
Ethanol (E)	24.7 ± 3.0 ^{a}	1.9 ± 0.1 ^{c}	1602 ± 66 ^{a}
E:W 90:10	24.0 ± 5.2 ^{ab}	2.1 ± 0.7 ^{bc}	1484 ± 28 ^{ab}
E:AA 90:10	25.9 ± 3.6 ^{a}	2.7 ± 0.9 ^{abc}	1481 ± 64 ^{ab}
E:AA 80:20	30.8 ± 3.5 ^{a}	5.9 ± 0.6 ^{abc}	1138 ± 129 ^{de}
E:AA 70:30	27.3 ± 2.8 ^{a}	3.7 ± 0.8 ^{abc}	1176 ± 63 ^{cd}
IPA:AA 80:20	30.4 ± 9.5 ^{a}	4.9 ± 1.7 ^{abc}	1226 ± 213 ^{bcd}

Ethanol produced the highest mean Young's modulus (1602 MPa), although this value was not statistically different from those obtained with pure acetic acid, E:W 90:10, or E:AA 90:10. The ethanol-cast film also exhibited low elongation at break and moderate tensile strength, indicating a stiff and poorly extensible mechanical response. This is in line with earlier reports that neat-ethanol-cast EC films can achieve good baseline mechanical performance without plasticizer [5,8], but combine this with limited extensibility.

Acetic acid and the E:AA blends exhibited a distinct mechanical profile. Pure acetic acid provided the highest elongation at break while maintaining high tensile strength and a moderate modulus, indicating a comparatively strong and extensible mechanical response. This behavior suggests that acetic acid may promote favorable EC chain organization during film formation, consistent with the broader influence of solvent–polymer interactions reported for other solution-cast polymer systems [22]. Similarly, E:AA 80:20 combined high mean tensile strength and elongation with a comparatively low modulus and the lowest mean WVTR. This response may result from the combined influence of acetic acid–EC interactions, evaporation kinetics, and residual acetic acid within the matrix.

SEM surface micrographs of the E:W 90:10 and E:AA 80:20 films showed continuous surfaces without obvious micron-scale cracks or open pores at the magnifications examined (Figure S2). The E:W 90:10 film exhibited a comparatively smooth surface, while the E:AA 80:20 film showed a somewhat greater number of isolated surface irregularities; however, the overall morphological difference was modest. Consequently, the lower mean WVTR of E:AA 80:20 cannot be directly attributed to the elimination of visible surface defects, and the present surface SEM images do not demonstrate denser molecular packing or reduced bulk porosity. Selected stress–strain curves for the solvent series are shown in Figure S4 and are consistent with the tensile-property trends summarized in Table 4.

3.3. Effect of Plasticizer Addition on the Barrier, Surface, and Mechanical Properties of EC Films

Although E:AA 80:20 produced the lowest mean WVTR and a favorable mechanical profile, E:W (90:10) was selected as the model solvent system for the additive studies because it represents a widely used EC casting system and provided a practical baseline for comparing the effects of plasticizers and nanofillers under a common formulation condition. Accordingly, the effect of seven plasticizers (glycerol, sorbitol, triacetin, tributyl citrate, dimethyl sebacate, dibutyl sebacate, and methyl oleate) was evaluated in EC solutions (M_n 47,000 g/mol) prepared in E:W (90:10) at concentrations of 0.1 and 1 wt.%, relative to the total mass of the film-forming solution, corresponding to 2 and 20 wt.% relative to EC, respectively. Although most of the plasticizers evaluated are relatively low-volatility compounds under the drying conditions used, differences in volatility and affinity for the EC matrix may have resulted in different degrees of plasticizer retention during the 16 h drying step at 50 °C. Since the actual plasticizer content of the dried films was not quantified, this potential contribution to the observed formulation-dependent behavior cannot be excluded.

The unplasticized film exhibited a relatively low WVTR (ca. 314 g/(m^2·day)), comparable to or slightly higher than those obtained with certain hydrophobic ester plasticizers at 1 wt.% loading, namely methyl oleate (ca. 301 g/(m^2·day)) and tributyl citrate (ca. 266 g/(m^2·day)), Figure 5. Tributyl citrate produced the lowest mean WVTR among all formulations; however, this value was not statistically different from that of the unplasticized control. These results indicate that selected hydrophobic ester plasticizers, particularly methyl oleate and tributyl citrate at 1 wt.%, can be incorporated without significantly increasing WVTR under the tested conditions. By contrast, the polyol plasticizers glycerol and sorbitol produced some of the highest mean WVTR values, consistent with their hydrophilic and highly water-miscible nature. Such plasticizers are known to disrupt intermolecular interactions within the polymer network and increase the availability of water-accessible domains, thereby facilitating moisture transport. Glycerol has also been reported to increase water vapor transmission to a greater extent than sorbitol in polysaccharide-based films, owing to its stronger plasticizing effect and greater disruption of polymer–polymer interactions [23]. The remaining hydrophobic ester plasticizers (triacetin, dimethyl sebacate and dibutyl sebacate) presented intermediate WVTR values, generally close to those of the unplasticized control. Overall, the observed distinction between hydrophobic ester plasticizers and polyols is consistent with previous reports identifying citrate- and sebacate-based esters as effective low-permeability plasticizers for EC coatings [8].

Plasticizer formulation significantly affected the apparent WCA, but no systematic concentration-dependent trend was observed, Figure 6. Most plasticizer-containing films exhibited intermediate WCA values and were not significantly different from the unplasticized control (71.9 ± 4.7°). The lowest mean WCA was obtained with 1 wt.% triacetin (66.0 ± 1.9°), which was significantly lower than 0.1 wt.% triacetin (78.8 ± 3.9°), 0.1 wt.% glycerol (79.4 ± 2.2°) and 1 wt.% dimethyl sebacate (80.5 ± 1.7°). These results indicate that the effect of plasticizer addition on surface wettability depended on plasticizer chemistry and concentration rather than following a general increase or decrease in WCA with plasticizer loading.

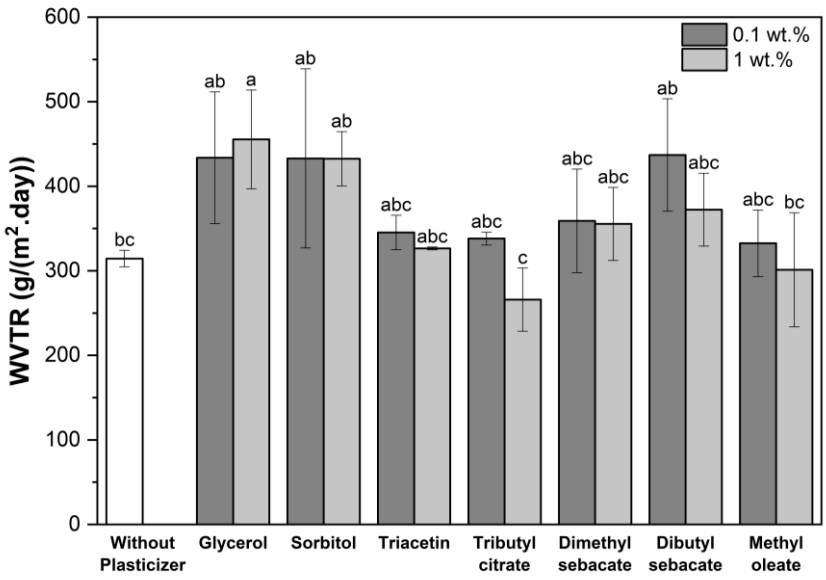


Figure 5. Water vapor transmission rate (WVTR) of EC films (5 wt.%, M_n 47,000 g/mol, E:W 90:10) containing 0.1 wt.% (gray) and 1 wt.% (light gray) of plasticizers. Results are presented as mean ± standard deviation (n = 3). Different letters above the bars indicate statistically significant differences between formulations according to one-way ANOVA followed by Tukey's HSD post hoc test ($p < 0.05$).

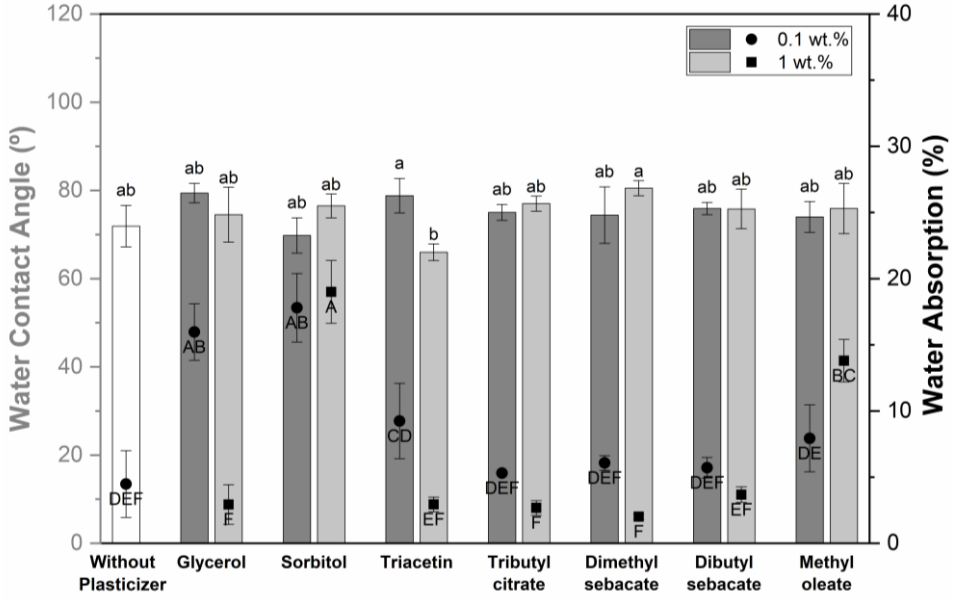


Figure 6. Water contact angle (bars, left axis) and water absorption (●, 0.1 wt.%; ■, 1 wt.%, right axis) of EC films (5 wt.%, M_n 47,000 g/mol, E:W 90:10) containing 0.1 wt.% (gray) and 1 wt.% (light gray) of plasticizers. Results are expressed as mean ± standard deviation (n = 3). Different letters indicate statistically significant differences within each property according to one-way ANOVA followed by Tukey's HSD post hoc test ($p < 0.05$). Water contact angle and water absorption were analyzed independently.

Water absorption showed a distinct dependence on plasticizer type and concentration. Sorbitol showed distinctive behavior, maintaining a high WA at both concentrations (ca. 18–19%). This may be related to its tendency to form less mobile, crystalline or phase-separated domains within the matrix rather than acting as a uniformly dispersed plasticizer, thereby sustaining water uptake despite changes in concentration [24]. In contrast, glycerol showed the opposite trend, with WA decreasing markedly from 0.1 to 1 wt.%. Although glycerol is generally more hydrophilic than sorbitol and is often associated with increased

moisture uptake in polysaccharide films [25], the substantial reduction observed at 1 wt.% suggests that, at higher loading, glycerol may be more effectively and homogeneously incorporated within the matrix, thereby limiting water uptake relative to that observed at lower concentrations. These findings highlight that WA is governed not only by plasticizer hydrophilicity, but also by its distribution and interactions within the polymer network. Methyl oleate showed low WA at 0.1 wt.% but a marked increase at 1 wt.%. This concentration-dependent response may reflect differences in its compatibility or distribution within the EC matrix, although the underlying mechanism cannot be established from the present data. The remaining hydrophobic esters (triacetin, tributyl citrate, dimethyl sebacate and dibutyl sebacate) showed consistently low WA values that decreased further at 1 wt.% loading, suggesting good compatibility with the EC matrix and limited promotion of water-accessible pathways [8].

The nominal plasticizer concentration of 0.1 wt.% in the film-forming solution corresponded to 2 wt.% relative to EC. At this loading, glycerol and sorbitol produced significantly higher tensile-strength values (41.9 and 48.6 MPa, respectively) than the unplasticized control (24.0 MPa), Table 5. Sorbitol also produced a significantly higher Young's modulus (1992 MPa) than the control (1484 MPa), whereas the modulus of the glycerol-containing film (1704 MPa) was not statistically different from that of the control. The simultaneous increase in tensile strength and stiffness observed for sorbitol is consistent with an antiplasticization-like response. Antiplasticization is a well-documented phenomenon in glassy polymers in which relatively low plasticizer concentrations may increase stiffness or strength, potentially by promoting more efficient molecular packing before the conventional free-volume-driven plasticization effect becomes dominant at higher loadings [26]. Glycerol showed a partial antiplasticization-like response, characterized by a significant increase in tensile strength without a statistically significant change in Young's modulus.

Table 5. Tensile strength, elongation at break, and Young's modulus of EC films (5 wt.%, M_n 47,000 g/mol, E:W 90:10) with different plasticizers. Results are expressed as mean ± standard deviation (n = 3). Different lowercase superscript letters within the same column indicate statistically significant differences between formulations according to one-way ANOVA followed by Tukey's HSD post hoc test ($p < 0.05$).

Plasticizer		Tensile Strength (MPa)	Elongation at Break (%)	Young's Modulus (MPa)
Without plasticizer		24.0 ± 5.2^{bcd}	2.1 ± 0.7^{c}	1484 ± 28^{bc}
Glycerol	0.1 wt.%	41.9 ± 4.7^{a}	5.7 ± 2.2^{ab}	1704 ± 84^{b}
	1 wt.%	14.6 ± 4.9^{defgh}	1.6 ± 0.6^{c}	1030 ± 83^{ef}
Sorbitol	0.1 wt.%	48.6 ± 1.7^{a}	4.7 ± 0.5^{bc}	1992 ± 102^{a}
	1 wt.%	25.4 ± 3.0^{bc}	3.0 ± 0.6^{bc}	1232 ± 53^{de}
Triacetin	0.1 wt.%	13.2 ± 0.7^{efghi}	1.8 ± 0.1^{c}	938 ± 56^{fg}
	1 wt.%	4.1 ± 3.1^{i}	2.5 ± 0.8^{c}	353 ± 161^{i}
Tributyl citrate	0.1 wt.%	29.8 ± 3.1^{b}	7.8 ± 0.6^{a}	1353 ± 21^{cd}
	1 wt.%	6.4 ± 1.1^{hi}	2.5 ± 0.7^{bc}	598 ± 79^{hi}
Dimethyl sebacate	0.1 wt.%	21.5 ± 2.5^{bcdef}	4.0 ± 1.1^{bc}	1209 ± 103^{de}
	1 wt.%	7.5 ± 1.0^{ghi}	2.2 ± 0.4^{c}	605 ± 123^{hi}
Dibutyl sebacate	0.1 wt.%	17.5 ± 3.1^{cdefg}	1.7 ± 0.5^{c}	1409 ± 148^{cd}
	1 wt.%	7.5 ± 1.6^{ghi}	2.9 ± 0.1^{bc}	602 ± 20^{hi}
Methyl oleate	0.1 wt.%	22.1 ± 5.5^{bcde}	4.2 ± 2.1^{bc}	1184 ± 60^{de}
	1 wt.%	11.8 ± 3.6^{fghi}	4.9 ± 2.0^{abc}	745 ± 57^{gh}

At 1 wt.% in the film-forming solution, corresponding to 20 wt.% relative to EC, all plasticizers produced lower mean tensile-strength and Young's-modulus values than those obtained at 0.1 wt.%. Young's modulus was significantly lower than that of the unplasticized control for all plasticizers, whereas the statistical significance of the tensile-strength reduction depended on plasticizer type. In particular, the tensile-strength values of the glycerol- and sorbitol-containing films were not statistically different from that of the control, while triacetin, tributyl citrate, dimethyl sebacate, dibutyl sebacate, and methyl oleate produced significantly lower values. This overall response is consistent with conventional plasticization at higher loading, in which increased chain mobility and free volume reduce the stiffness and load-bearing capacity of the polymer matrix [5,8,26]. Triacetin produced the lowest mean tensile strength and Young's modulus at 1 wt.% (4.1 and 353 MPa, respectively), indicating a pronounced softening and weakening effect in the EC/E:W 90:10 matrix. However, plasticizer compatibility and phase morphology were not directly evaluated and therefore cannot be established from the mechanical data alone.

Analysis of elongation at break showed that tributyl citrate and glycerol at 0.1 wt.% produced significantly higher values (7.8 and 5.7%, respectively) than the unplasticized control (2.1%). Tributyl citrate combined increased elongation with a tensile-strength value that was not significantly different from that of the control, consistent with the reported compatibility of citrate esters with EC [8]. Glycerol also increased elongation while producing a significantly higher tensile-strength value (42 MPa vs. 30 MPa for tributyl citrate), and its elongation was not statistically different from that of tributyl citrate (5.7 vs. 7.8%); by the same statistical criteria used elsewhere in this study, glycerol and tributyl citrate should therefore be regarded as jointly, rather than individually, offering the most favorable strength–elongation combination at 0.1 wt.%. At 1 wt.%, none of the plasticizer-containing films exhibited an elongation-at-break value statistically different from that of the control, despite the significant reduction in Young's modulus observed for all formulations. Methyl oleate presented the highest mean elongation at this concentration (4.9%), but this value was not statistically different from that of the control. Together with its higher mean WA, this numerical trend may reflect concentration-dependent changes in plasticizer distribution; however, phase separation was not directly demonstrated.

ATR-FTIR spectra were acquired for representative films containing glycerol, sorbitol, triacetin and tributyl citrate at 0.1 and 1 wt.% (Figure S5). All plasticized films retained the characteristic EC fingerprint [5]. For the ester plasticizers, triacetin and tributyl citrate, an additional contribution in the carbonyl region around 1700–1750 cm^{-1} was evident, particularly at the higher loading, consistent with the presence of these additives within the film [27]. Glycerol- and sorbitol-containing films showed only subtle changes in the hydroxyl and fingerprint regions and no new bands indicative of chemical reaction with EC. Overall, the FTIR results are consistent with physical plasticization and intermolecular interactions rather than formation of new covalent bonds. They do not, by themselves, distinguish antiplasticization from other physical organization effects. Selected stress–strain curves (Figure S6) visually support the strong concentration dependence of the mechanical response, including the high-stress response of the low-loading glycerol/sorbitol systems and the pronounced softening of the 1 wt.% triacetin formulation.

3.4. Effect of Nanofiller Type and Loading on the Barrier, Surface, and Mechanical Properties of EC Nanocomposite Films

Using EC (M_n 47,000 g/mol) dissolved in E:W 90:10, CNC, CNF, SiO_2, and ZnO were evaluated at concentrations of 0.1 and 0.5 wt.% relative to the total mass of the film-forming solution. Since the EC concentration was 5 wt.%, these concentrations corresponded to nanofiller loadings of 2 and 10 wt.% relative to EC, respectively. Because the fillers have substantially different densities, their estimated volume fractions in the dried EC nanocom-

posites also differed, ranging from approximately 0.4 to 1.5 vol.% at the lower formulation loading and from approximately 2.0 to 7.1 vol.% at the higher loading. No significant differences in WVTR were observed between the control and the nanofiller-containing films, regardless of nanofiller type or concentration, Figure 7. Therefore, the absence of a statistically detectable barrier effect cannot be attributed simply to insufficient nanofiller concentration. Instead, the response may depend on nanofiller dispersion, particle aggregation, surface chemistry, compatibility with EC, and the resulting film morphology, which collectively determine whether an effective tortuous diffusion pathway is formed [28]. In a previous study, the incorporation of 2.5 wt.% unmodified nanofibrillated cellulose into ethanol-cast EC films increased WVTR relative to neat EC [11]. Since this loading lies between the two nanofiller loadings evaluated in the present work, the contrasting results further indicate that concentration alone does not determine the effect of nanofillers on water-vapor transport.

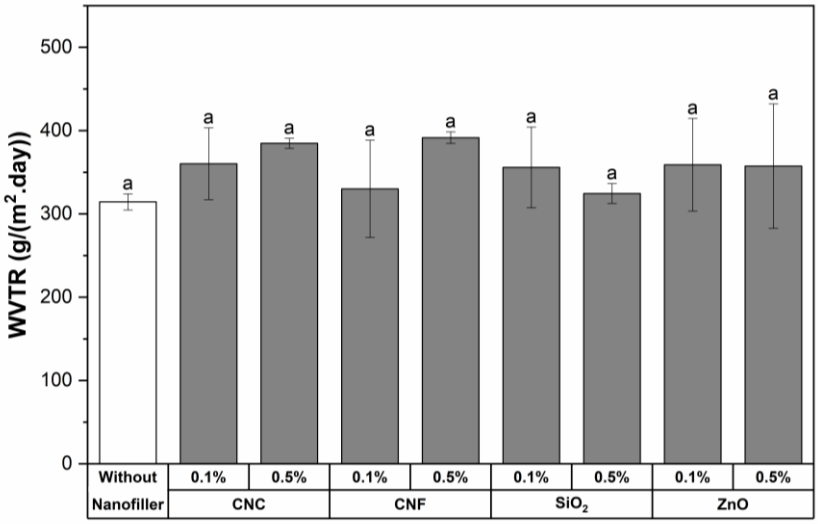


Figure 7. Water vapor transmission rate (WVTR) of EC films (5 wt.%, M_n 47,000 g/mol, E:W 90:10) containing nanofiller at 0.1 and 0.5 wt.%. Results are presented as mean ± standard deviation (n = 3). Different lowercase letters above the bars indicate statistically significant differences between formulations according to one-way ANOVA followed by Tukey's HSD post hoc test ($p < 0.05$).

Nanofiller type and loading did not significantly affect the apparent WCA, Figure 8. Mean values ranged from 71.6 ± 5.0° to 82.9 ± 5.4°, and all formulations belonged to the same Tukey group. The highest numerical values were observed for 0.5 wt.% ZnO (82.9 ± 5.4°) and 0.5 wt.% SiO_2 (81.8 ± 7.8°), but neither differed significantly from the unfilled EC control (71.9 ± 4.7°). The observed variations should therefore be interpreted as numerical trends rather than statistically demonstrated changes in surface wettability. In particular, the present data do not support a concentration-dependent WCA effect for SiO_2 or ZnO.

Regarding WA, the film containing 0.5 wt.% CNF exhibited the highest value (ca. 27%) among the tested formulations, Figure 8. The SEM surface images did not reveal the same pronounced micron-scale clustering observed for some of the other fillers; therefore, the high WA should not be attributed solely to large surface aggregates. Instead, it may be associated with the intrinsic hydrophilicity of unmodified CNF, arising from the abundant hydroxyl groups at the cellulose surface [29], together with possible CNF-rich domains and/or interfacial regions within the EC matrix. The hydrophilic nature of unmodified nanocellulose and the influence of its dispersion and interfacial compatibility on the behavior of EC/nanocellulose composites have also been reported previously [11]. This behavior was not accompanied by a significant change in WVTR, indicating that, under the present

conditions, the increased water uptake did not result in a statistically detectable increase in water-vapor transmission.

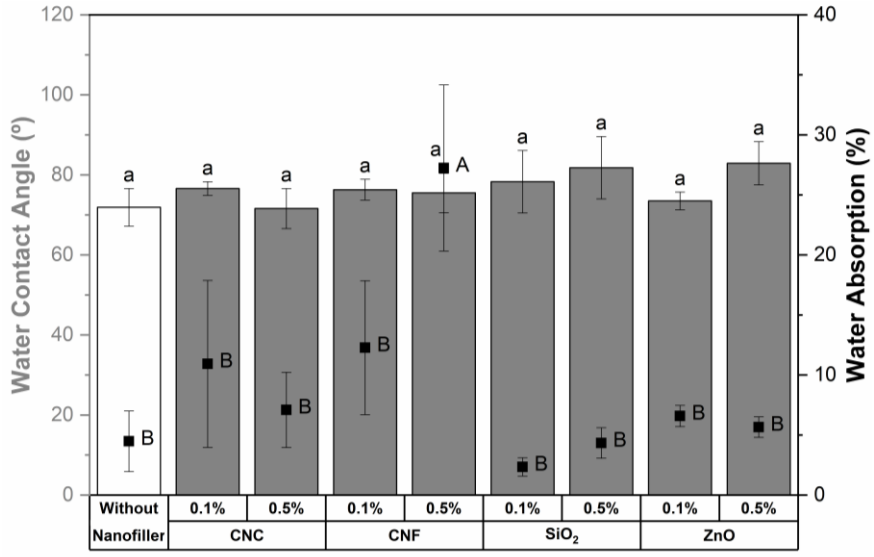


Figure 8. Water contact angle (bars, left axis) and water absorption (■, right axis) of EC films (5 wt.%, M_n 47,000 g/mol, E:W 90:10) containing nanofiller at 0.1 and 0.5 wt.%. Results are expressed as mean ± standard deviation (n = 3). Different letters indicate statistically significant differences within each property according to one-way ANOVA followed by Tukey's HSD post hoc test ($p < 0.05$). Water contact angle and water absorption were analyzed independently.

Both CNC- and CNF-containing films presented lower mean tensile-strength values than the unfilled control, with the largest numerical decreases observed at 0.5 wt.% loading, Table 6. Mean Young's-modulus values were also lower than that of the control, although no consistent concentration-dependent trend was observed, particularly for CNF. However, according to the Tukey groupings, none of these values was statistically different from that of the control. Although both nanomaterials are cellulose-based, their highly hydroxylated surfaces contrast with the less polar and more hydrophobic nature of EC, which may limit compatibility between phases. In addition, nanocellulose may aggregate during processing, creating stress-concentration points that can compromise the mechanical performance of the films. Similar behavior has been reported in EC/nanocellulose composites, where poor interfacial adhesion and particle agglomeration resulted in lower strength and stiffness than neat EC [11].

In contrast, SiO_2- and ZnO-containing films produced the highest mean values for selected mechanical properties, although these values were not statistically different from those of the unfilled control. ZnO produced the highest mean tensile-strength values at both concentrations (ca. 32–33 MPa) and the highest elongation at break at 0.1 wt.% (3.3%). These results indicate a numerical tendency toward higher strength and elongation rather than a statistically demonstrated improvement. Such trends may be associated with stress transfer between the nanoparticles and the EC matrix and with favorable interfacial interactions, as reported for ZnO nanoparticles in other polymer films [30]. For SiO_2, increasing the nanofiller concentration from 0.1 to 0.5 wt.% produced numerically higher tensile strength and Young's modulus. However, neither formulation differed significantly from the unfilled control, and a concentration-dependent reinforcing effect therefore cannot be established from the present data.

The ATR-FTIR spectra of the 0.5 wt.% nanocomposites retained the dominant EC fingerprint (Figure S8) [5]. The CNC- and CNF-containing films showed extensive spectral overlap with the EC matrix, as expected from their chemically related cellulose-based

structures [11]. The SiO_2- and ZnO-containing films showed additional changes in the fingerprint/low-wavenumber region consistent with the characteristic Si–O–Si and Zn–O vibrations reported for these inorganic phases [31,32]. However, no new strong bands attributable to covalent bonding between the fillers and EC were observed. The systems should therefore be described as physically dispersed EC nanocomposites rather than as molecularly dissolved mixtures.

Table 6. Tensile strength, elongation at break, and Young's modulus of EC films (5 wt.%, M_n 47,000 g/mol, E:W 90:10) containing different nanofillers. Results are expressed as mean ± standard deviation (n = 3). Different lowercase superscript letters within the same column indicate statistically significant differences between formulations according to one-way ANOVA followed by Tukey's HSD post hoc test ($p < 0.05$).

Nanofiller		Tensile Strength (MPa)	Elongation at Break (%)	Young's Modulus (MPa)
Without nanofiller		24.0 ± 5.2 ^{abc}	2.1 ± 0.7 ^{ab}	1484 ± 28 ^{ab}
CNC	0.1 wt.%	18.3 ± 8.4 ^{bc}	2.3 ± 0.1 ^{ab}	1441 ± 258 ^{b}
	0.5 wt.%	15.5 ± 2.1 ^{c}	1.2 ± 0.1 ^{b}	1381 ± 73 ^{b}
CNF	0.1 wt.%	19.0 ± 1.7 ^{abc}	1.9 ± 0.2 ^{b}	1225 ± 152 ^{b}
	0.5 wt.%	15.4 ± 2.3 ^{c}	1.3 ± 0.1 ^{b}	1405 ± 120 ^{b}
SiO_2	0.1 wt.%	27.5 ± 5.2 ^{abc}	2.2 ± 0.7 ^{ab}	1574 ± 48 ^{ab}
	0.5 wt.%	31.5 ± 5.3 ^{ab}	2.0 ± 0.4 ^{ab}	1871 ± 105 ^{a}
ZnO	0.1 wt.%	33.3 ± 6.1 ^{a}	3.3 ± 1.1 ^{a}	1556 ± 79 ^{ab}
	0.5 wt.%	32.4 ± 8.0 ^{a}	2.2 ± 0.5 ^{ab}	1817 ± 177 ^{a}

SEM revealed clear filler-dependent differences in surface morphology (Figure S7). The unfilled EC film was comparatively smooth and homogeneous. The CNC-containing film showed marked heterogeneity with micron-scale clustered features consistent with incomplete dispersion/agglomeration. The CNF-containing film remained comparatively homogeneous, with only sparse isolated nodular or elongated features. SiO_2 produced numerous particulate clusters, while ZnO generated the most pronounced surface heterogeneity and larger irregular clustered domains. Because no elemental mapping was performed, these features are most appropriately described as regions consistent with filler-rich agglomerates rather than being assigned unequivocally to individual particles. The use of higher-energy dispersion methods, such as ultrasonication or high-shear homogenization, could potentially reduce agglomeration and improve filler distribution. Ultrasonication, in particular, has been widely used to promote CNC dispersion, although its effectiveness depends strongly on the applied energy and processing conditions [33]. Improved dispersion could modify the mechanical and barrier response of the nanocomposites; however, the magnitude and direction of these effects cannot be predicted from the present data, since they also depend on filler–matrix compatibility and processing conditions. The visible clustering, particularly for CNC, SiO_2 and ZnO, provides a plausible explanation for the absence of a statistically significant WVTR improvement, because aggregation can reduce the effectiveness of a uniformly distributed tortuous diffusion pathway. However, the comparatively high mean mechanical values of the SiO_2- and ZnO-containing films, despite their visible surface heterogeneity, also show that no simple one-to-one relationship between surface dispersion and tensile performance can be established from the present data. Selected stress–strain curves are provided in Figure S9.

To evaluate whether the apparent WCA values were substantially influenced by short-time wetting/spreading, the contact angle was additionally examined immediately after droplet deposition and after 1 and 5 s for all formulation series (Tables S3–S6). Across the

evaluated films, the change between 0 and 5 s was small, remaining within ±2°, and was generally comparable to the experimental variability. This indicates limited short-time spreading during the 5 s acquisition window. The influence of droplet volume was also examined using 2, 4 and 6 µL droplets on two representative EC films. No significant differences were detected among the three volumes within either film (Table S2), supporting the use of a 6 µL droplet under the present measurement conditions.

Film thickness varied among formulations, with mean values ranging from approximately 0.06 to 0.18 mm (Table S7). Since WVTR is thickness-dependent, these differences may have contributed to the measured water-vapor transmission rates. However, no consistent inverse relationship between film thickness and WVTR was apparent across the formulation series. For example, the IPA-cast film exhibited one of the highest mean thicknesses (0.17 mm) while also showing the highest mean WVTR, whereas E:AA 80:20 had a lower thickness (0.12 mm) and the lowest mean WVTR among the solvent systems. Similarly, substantial thickness variation among the commercial EC grades was not accompanied by a corresponding systematic variation in WVTR. These observations suggest that thickness alone does not explain the formulation-dependent WVTR behavior. Film density and bulk porosity were not quantified in the present study and may also contribute to water-vapor transport; therefore, their influence cannot be independently resolved from the present data.

To place the present results in a practical food-packaging context, the thickness, mechanical properties, and WVTR of the developed EC films were compared with selected cellulose-based films and a commercial flexible packaging material (Table 7). The selected benchmarks include neat and nanocellulose-reinforced EC films, an all-cellulose CNF film, and a commercial metallized BOPP film used for food-packaging applications. Where available, film thickness and the corresponding WVTR test conditions are reported to facilitate interpretation of the differences between materials.

Table 7. Contextual comparison of the thickness, mechanical properties, and water vapor transmission rate (WVTR) of the ethyl cellulose films developed in the present study with selected cellulose-based and commercial packaging materials. Reported WVTR values are accompanied by the corresponding test method and environmental conditions, where available. Values are provided for contextual purposes only and should not be interpreted as directly equivalent because of differences in material structure, film thickness, processing history, temperature, relative-humidity gradient, and measurement method.

Material/Benchmark	Thickness (µm)	Tensile Strength (MPa)	Elongation at Break (%)	WVTR (g/(m^2·Day))	WVTR Method and Conditions	Ref.
EC films—present study	60–180	4–49	1–10	266–461	Adapted ASTM E96, water method; 32 °C, 50% RH	This study
Neat EC film	29.0 ± 4.9	10.1 ± 1.2	1.6 ± 0.3	250 ± 43	ASTM E96/E96M, desiccant method; 25 °C, 80% RH	[11]
EC/mNFC-LA nanocomposite	27.5 ± 4.5	23.2 ± 0.8	2.8 ± 0.4	31 ± 20	ASTM E96/E96M, desiccant method; 25 °C, 80% RH	[11]
All-cellulose CNF7 film	43 ± 2	83.9 ± 1.5	7.8 ± 1.1	44.7 ± 3.0	Modified ASTM E96/E96M; 25 °C, 75% RH	[34]
Torayfan® PL2 metallized BOPP film	15	100/300 [1]	200/60 [1]	0.16	ASTM F1249; 38 °C, 90% RH	[35]

[1] MD/TD: machine direction/transverse direction.

The comparison indicates that the mechanical performance of the present EC films overlaps with the range reported for laboratory-scale cellulose-based films, with some formulations reaching tensile strengths comparable to or higher than neat EC reported in the literature. In contrast, the water-vapor barrier performance remains substantially lower than that of optimized EC/nanocellulose films and commercial metallized BOPP packaging. This comparison therefore highlights water-vapor barrier improvement as a key priority for further development of the present EC formulations toward demanding food-packaging applications.

As a food-specific application benchmark, the UNICEF specification for fortified biscuits intended for extended shelf life requires primary packaging with a WVTR below 1.5 g/(m^2·day) at 38 °C and 90% RH, determined according to ASTM F1249-13 or an equivalent method [36]. Compared with the WVTR values obtained for the present EC films (approximately 266–461 g/(m^2·day)), this requirement illustrates the substantially greater moisture-barrier performance needed for long-shelf-life, moisture-sensitive dry-food applications.

Nevertheless, the numerical values in Table 7 and the food-specific benchmark should be interpreted contextually rather than as directly equivalent performance ratios, since WVTR is strongly influenced by film thickness, temperature, relative-humidity gradient, test configuration, and measurement method. Mechanical properties are likewise affected by material structure, orientation, thickness, and testing conditions.

4. Conclusions

This study comparatively evaluated the effects of commercial grade and apparent molecular weight, solvent system, plasticizer type and concentration, and nanofiller type and concentration on the performance of solvent-cast EC films prepared under a common formulation platform (5 wt.% EC). Among the variables investigated, solvent selection produced clear formulation-dependent differences in WVTR. Acetic acid-containing systems, particularly E:AA 80:20, produced films combining the lowest mean WVTR with high tensile strength and elongation, identifying them as promising solvent systems for further optimization.

Plasticizer formulation produced the largest variation in mechanical performance. Tributyl citrate and glycerol at 0.1 wt.% provided the most favorable strength–elongation balance, whereas formulations containing 1 wt.% plasticizer generally exhibited lower stiffness and lower mean tensile strength. Sorbitol significantly increased both tensile strength and stiffness at low loading, whereas glycerol significantly increased tensile strength without a significant change in Young's modulus. Across the commercial EC grades, no consistent monotonic relationship was observed between apparent M_n^{SEC} and WVTR, WA, surface wettability, or mechanical performance. Because the evaluated grades originated from different manufacturers and may differ in molecular-weight distribution, degree and pattern of substitution, and manufacturing history, the independent effect of molecular weight cannot be isolated from the present dataset.

Under the dispersion conditions employed, nanofiller addition did not produce statistically significant improvements in WVTR, WCA, or tensile properties relative to the unfilled control. Nevertheless, filler type and loading influenced water absorption and surface morphology, while SEM revealed filler-dependent heterogeneity and clustering, particularly for CNC, SiO_2, and ZnO. These results highlight the importance of dispersion quality and filler–matrix compatibility in the further development of EC nanocomposites.

The present work should be regarded as a preliminary formulation screening. Each formulation was prepared from a single film casting; therefore, the reported replicates represent within-film technical replicates and do not establish film-to-film or batch-to-batch repro-

ducibility. In addition, formulation variables were screened individually, and film density, bulk porosity, residual solvent, and filler distribution through the complete film thickness were not quantified. Future work should therefore prioritize independent replicate-film validation of the most promising formulations, followed by combined-variable optimization and complementary structural, thermal, and dynamic-mechanical characterization.

Supplementary Materials: The following supporting information can be downloaded at https://www.mdpi.com/article/10.3390/j9040033/s1, Table S1. Supplier-reported technical specifications of the CNC, CNF, ZnO, and SiO_2 nanofillers used in this study (Nanografi). Table S2. Water contact angle (WCA) of ethyl cellulose films with different molecular weights, determined using droplet volumes of 2, 4 and 6 µL. Results are expressed as mean ± standard deviation (n = 3). No significant differences were detected among 2, 4 and 6 µL droplets within either representative EC grade (one-way ANOVA followed by Tukey HSD, α = 0.05). Table S3. Water contact angle (WCA) of ethyl cellulose films with different molecular weights, measured immediately after droplet deposition (t = 0 s) and after 1 and 5 s. Results are expressed as mean ± standard deviation (n = 3). ΔWCA_{5-0s} was calculated as the difference between the mean WCA measured at 5 s and at 0 s. Table S4. Water contact angle (WCA) of 5 wt.% Ethocel 45 films prepared using different solvents and solvent mixtures, measured immediately after droplet deposition (t = 0 s) and after 1 and 5 s. Results are expressed as mean ± standard deviation (n = 3). ΔWCA_{5-0s} was calculated as the difference between the mean WCA measured at 5 s and at 0 s. Table S5. Water contact angle (WCA) of 5 wt.% Ethocel 45 films containing different plasticizers at 0.1 and 1 wt.%, measured immediately after droplet deposition (t = 0 s) and after 1 and 5 s. Results are expressed as mean ± standard deviation (n = 3). ΔWCA_{5-0s} was calculated as the difference between the mean WCA measured at 5 s and at 0 s. Table S6. Water contact angle (WCA) of ethyl cellulose films containing different nanofillers at 0.1 and 0.5 wt.%, measured immediately after droplet deposition (t = 0 s) and after 1 and 5 s. Results are expressed as mean ± standard deviation (n = 3). ΔWCA_{5-0s} was calculated as the difference between the mean WCA measured at 5 s and at 0 s. Figure S1. Selected tensile stress–strain curves of 5 wt.% ethyl cellulose films with different molecular weights (18,000–104,200 g mol^{-1}), prepared by solvent casting using an ethanol/water (90:10, v/v) solvent system. Figure S2. SEM surface micrographs of 5 wt.% Ethocel 45 films prepared by solvent casting using ethanol:water (E:W, 90:10, v/v) and ethanol:acetic acid (E:AA, 80:20, v/v), recorded at 1000×, 5000×, and 10,000× magnification. Figure S3. Normalized FTIR spectra of 5 wt.% Ethocel 45 films prepared by solvent casting using ethanol:water (E:W, 90:10, v/v) and ethanol:acetic acid (E:AA, 80:20, v/v). Figure S4. Selected tensile stress–strain curves of 5 wt.% Ethocel 45 films prepared using different solvents and solvent mixtures. Figure S5. Normalized FTIR spectra of 5 wt.% Ethocel 45 films containing different plasticizers at 0.1 and 1 wt.%, prepared by solvent casting using ethanol:water (E:W, 90:10, v/v). Figure S6. Selected tensile stress–strain curves of 5 wt.% Ethocel 45 films containing different plasticizers at 0.1 and 1 wt.%, prepared by solvent casting using ethanol:water (E:W, 90:10, v/v). Figure S7. SEM surface micrographs of 5 wt.% Ethocel 45 films prepared by solvent casting using ethanol:water (E:W, 90:10, v/v) without nanofiller and containing 0.5 wt.% CNC, CNF, SiO_2, or ZnO, recorded at 1000×, 5000×, and 10,000× magnification. Figure S8. Normalized FTIR spectra of 5 wt.% Ethocel 45 films containing different nanofillers at 0.5 wt.%, prepared by solvent casting using ethanol:water (E:W, 90:10, v/v). Figure S9. Selected tensile stress–strain curves of 5 wt.% Ethocel 45 films containing different nanofillers at 0.1 and 0.5 wt.%, prepared by solvent casting using ethanol:water (E:W, 90:10, v/v); Table S7. Thickness of ethyl cellulose (EC) films (5 wt.%) prepared with different molecular weights, solvent systems, plasticizers, and nanofillers. Results are expressed as mean (n = 3).

Author Contributions: Conceptualization, E.M.; methodology, E.M. and A.S.R.O.; validation, E.M. and A.A.S.A.; investigation, A.S.R.O. and D.F.; resources, F.E.A.; writing—original draft preparation, E.M.; writing—review and editing, A.S.R.O., D.F., A.A.S.A., and F.E.A.; supervision, F.E.A.; project administration, F.E.A.; funding acquisition, F.E.A. All authors have read and agreed to the published version of the manuscript.

Funding: This research was funded by COMPETE 2030, Portugal 2030, and the European Union, through the project SEA-FILM: Development of Flexible Ethyl cellulose Films for Biopackaging with Self-Degradation in Sea Water (No. 18286).

Institutional Review Board Statement: Not applicable.

Informed Consent Statement: Not applicable.

Data Availability Statement: The data presented in this study are available within the article and its Supplementary Materials.

Acknowledgments: The authors acknowledge IFF for providing selected Ethocel™ grades used in this study.

Conflicts of Interest: All authors are employed by Science 351–Disruptive & Sustainable R&D Innovations, Lda., which holds the SEA-FILM project referenced in the Funding statement. In addition, IFF provided several of the commercial Ethocel™ grades evaluated in this study free of charge (see Acknowledgments). The authors declare that these relationships did not influence the design, conduct, analysis, or reporting of the research.

Abbreviations

The following abbreviations are used in this manuscript:

AA	Acetic acid
CNC	Cellulose nanocrystals
CNF	Cellulose nanofibrils
DS	Degree of substitution
E	Ethanol
EC	Ethyl cellulose
HPC	Hydroxypropyl cellulose
IPA	Isopropanol
M_n	Number-average molecular weight
MWD	Molecular weight distribution
NP	Nanoparticle
SEC	Size-exclusion chromatography
W	Water
WA	Water absorption
WCA	Water contact angle
WVTR	Water vapor transmission rate

References

1. Rekhi, G.S.; Jambhekar, S.S. Ethylcellulose-a Polymer Review. *Drug Dev. Ind. Pharm.* **1995**, *21*, 61–77. [CrossRef]
2. Wasilewska, K.; Winnicka, K. Ethylcellulose—A Pharmaceutical Excipient with Multidirectional Application in Drug Dosage Forms Development. *Materials* **2019**, *12*, 3386. [CrossRef] [PubMed]
3. Arwidsson, H.; Nicklasson, M. Application of Intrinsic Viscosity and Interaction Constant as a Formulation Tool for Film Coating. I. Studies on Ethyl Cellulose 10 Cps in Organic Solvents. *Int. J. Pharm.* **1989**, *56*, 187–193. [CrossRef]
4. Azoury, R.; Elkayam, R.; Friedman, M. Nuclear Magnetic Resonance Study of an Ethyl Cellulose Sustained-Release Delivery System I: Effect of Casting Solvent on Hydration Properties. *J. Pharm. Sci.* **1988**, *77*, 425–427. [CrossRef] [PubMed]
5. Horvat, G.; Žvab, K.; Knez, Ž.; Novak, Z. Simple, One-Pot Method for Preparing Transparent Ethyl Cellulose Films with Good Mechanical Properties. *Polymers* **2022**, *14*, 2399. [CrossRef] [PubMed]
6. Davidovich-Pinhas, M.; Barbut, S.; Marangoni, A.G. Physical Structure and Thermal Behavior of Ethylcellulose. *Cellulose* **2014**, *21*, 3243–3255. Erratum in *Cellulose* **2015**, *22*, 2137.. [CrossRef]
7. Su, X.; Yang, Z.; Tan, K.B.; Chen, J.; Huang, J.; Li, Q. Preparation and Characterization of Ethyl Cellulose Film Modified with Capsaicin. *Carbohydr. Polym.* **2020**, *241*, 116259. [CrossRef] [PubMed]
8. Hyppölä, R.; Husson, I.; Sundholm, F. Evaluation of Physical Properties of Plasticized Ethyl Cellulose Films Cast from Ethanol Solution Part I. *Int. J. Pharm.* **1996**, *133*, 161–170. [CrossRef]

9. Kangarlou, S.; Haririan, I. Physico-Mechanical Analysis of Free Ethylcellulose Films Plasticized with Incremental Weight Percents of Dibutyl Sebacate. *Iran. J. Pharm. Sci.* **2007**, *3*, 135–142.
10. Shi, J.; Liu, W.; Jiang, X.; Liu, W. Preparation of Cellulose Nanocrystal from Tobacco-Stem and Its Application in Ethyl Cellulose Film as a Reinforcing Agent. *Cellulose* **2020**, *27*, 1393–1406. [CrossRef]
11. Klayya, S.; Pripdeevech, P.; Bilotti, E.; Zhang, H.; Soykeabkaew, N. High Barrier Bio-Nanocomposite Films of Ethyl Cellulose Integrated with Modified Nanocellulose: Effect of Nanocellulose's Substituted Side Chains on Film Performance. *RSC Appl. Polym.* **2025**, *3*, 1244–1257. [CrossRef]
12. *ASTM E96/E96M*; Standard Test Methods for Water Vapor Transmission of Materials. ASTM International: West Conshohocken, PA, USA, 2016.
13. *ASTM D570-98*; Standard Test Method for Water Absorption of Plastics. ASTM International: West Conshohocken, PA, USA, 2018.
14. *ISO 62:2008*; Plastics—Determination of Water Absorption. International Organization for Standardization (ISO): Geneva, Switzerland, 2008.
15. *ASTM D5725-99*; Standard Test Method for Surface Wettability and Absorbency of Sheeted Materials Using an Automated Contact Angle Tester. ASTM International: West Conshohocken, PA, USA, 2020.
16. *ASTM D882-12*; Standard Test Method for Tensile Properties of Thin Plastic Sheeting. ASTM International: West Conshohocken, PA, USA, 2012.
17. Narisawa, S.; Yoshino, H.; Hirakawa, Y.; Noda, K. Porosity-Controlled Ethylcellulose Film Coating. II. Spontaneous Porous Film Formation in the Spraying Process and Its Solute Permeability. *Int. J. Pharm.* **1994**, *104*, 95–106. [CrossRef]
18. Andersson, H.; Hjärtstam, J.; Stading, M.; Von Corswant, C.; Larsson, A. Effects of Molecular Weight on Permeability and Microstructure of Mixed Ethyl-Hydroxypropyl-Cellulose Films. *Eur. J. Pharm. Sci.* **2013**, *48*, 240–248. [CrossRef] [PubMed]
19. Kim, D.; Elf, P.; Nilsson, F.; Hedenqvist, M.S.; Larsson, A. In-Depth Understanding of the Effect of the Distribution of Substituents on the Morphology and Physical Properties of Ethylcellulose: Molecular Dynamics Simulations Insights. *Biomacromolecules* **2024**, *25*, 4046–4062. [CrossRef] [PubMed]
20. Lang, J.; Wang, N.; Wang, X.; Wang, Y.; Chen, G.; Zhang, H. Applications of the Hansen Solubility Parameter for Cellulose. *Bioresources* **2021**, *16*, 7112. [CrossRef]
21. Anbukarasu, P.; Sauvageau, D.; Elias, A. Tuning the Properties of Polyhydroxybutyrate Films Using Acetic Acid via Solvent Casting. *Sci. Rep.* **2015**, *5*, 17884. [CrossRef] [PubMed]
22. Lv, Y.; Lin, Y.; Chen, F.; Li, F.; Shangguan, Y.; Zheng, Q. Chain Entanglement and Molecular Dynamics of Solution-Cast PMMA/SMA Blend Films Affected by Hydrogen Bonding between Casting Solvents and Polymer Chains. *RSC Adv.* **2015**, *5*, 44800–44811. [CrossRef]
23. Syarifuddin, A.; Haliza, N.; Izzah, N.; Tahir, M.M.; Dirpan, A. Physical, Mechanical, Barrier, and Optical Properties of Sodium Alginate/Gum Arabic/Gluten Edible Films Plasticized with Glycerol and Sorbitol. *Foods* **2025**, *14*, 1219. [CrossRef] [PubMed]
24. Gaudin, S.; Lourdin, D.; Le Botlan, D.; Ilari, J.L.; Colonna, P. Plasticisation and Mobility in Starch-Sorbitol Films. *J. Cereal Sci.* **1999**, *29*, 273–284. [CrossRef]
25. Sanyang, M.L.; Sapuan, S.M.; Jawaid, M.; Ishak, M.R.; Sahari, J. Effect of Plasticizer Type and Concentration on Tensile, Thermal and Barrier Properties of Biodegradable Films Based on Sugar Palm (*Arenga pinnata*) Starch. *Polymers* **2015**, *7*, 1106–1124. [CrossRef]
26. Mascia, L.; Kouparitsas, Y.; Nocita, D.; Bao, X. Antiplasticization of Polymer Materials: Structural Aspects and Effects on Mechanical and Diffusion-Controlled Properties. *Polymers* **2020**, *12*, 769. [CrossRef] [PubMed]
27. Hegyesi, D.; Sovány, T.; Berkesi, O.; Pintye-Hódi, K.; Regdon, G., Jr. Study of the Effect of Plasticizer on the Structure and Surface Characteristics of Ethylcellulose Free Films with FT-IR Spectroscopy. *Microchem. J.* **2013**, *110*, 36–39. [CrossRef]
28. Arora, A.; Padua, G.W. Nanocomposites in Food Packaging. *J. Food Sci.* **2010**, *75*, R43–R49. [CrossRef] [PubMed]
29. Moon, R.J.; Martini, A.; Nairn, J.; Simonsen, J.; Youngblood, J. Cellulose Nanomaterials Review: Structure, Properties and Nanocomposites. *Chem. Soc. Rev.* **2011**, *40*, 3941–3994. [CrossRef] [PubMed]
30. Yao, L.; Sun, H.; Yu, C.; Weng, Y. Enhanced Xylan/PVA Composite Films via Nano-ZnO Reinforcement for Sustainable Food Packaging. *Polymers* **2025**, *17*, 1080. [CrossRef] [PubMed]
31. Hadia, N.J.; Ng, Y.H.; Stubbs, L.P.; Torsæter, O. High Salinity and High Temperature Stable Colloidal Silica Nanoparticles with Wettability Alteration Ability for Eor Applications. *Nanomaterials* **2021**, *11*, 707. [CrossRef] [PubMed]
32. Spoială, A.; Ilie, C.-I.; Trușcă, R.-D.; Oprea, O.-C.; Surdu, V.-A.; Vasile, B.Ș.; Ficai, A.; Ficai, D.; Andronescu, E.; Diță, L.-M. Zinc Oxide Nanoparticles for Water Purification. *Materials* **2021**, *14*, 4747. [CrossRef] [PubMed]
33. Girard, M.; Vidal, D.; Bertrand, F.; Tavares, J.R.; Heuzey, M.-C. Evidence-Based Guidelines for the Ultrasonic Dispersion of Cellulose Nanocrystals. *Ultrason. Sonochem.* **2021**, *71*, 105378. [CrossRef] [PubMed]

34. Jadaun, S.; Siddiqui, S.; Punia Bangar, S. Development and Characterization of Rice Straw-Derived All-Cellulose Nanocomposite Films Reinforced with Cellulose Nanofibers Obtained via High-Intensity Ultrasonication and High-Shear Dispersion. *Sustain. Food Technol.* **2026**, *4*, 4226–4248. [CrossRef]
35. Toray Plastics (America), Inc. Torayfan® PL2 Product Data Sheet. Available online: https://www.toraytpa.com/wp-content/uploads/2019/06/TFN-PL2-Technical-Data-Sheet-Metric-1.pdf (accessed on 9 October 2026).
36. United Nations Children's Fund (UNICEF). Product Specification Sheet: Fortified Biscuits-CAR 200×50 g. Available online: https://www.unicef.org/supply/media/21011/file (accessed on 9 October 2026).

Disclaimer/Publisher's Note: The statements, opinions and data contained in all publications are solely those of the individual author(s) and contributor(s) and not of MDPI and/or the editor(s). MDPI and/or the editor(s) disclaim responsibility for any injury to people or property resulting from any ideas, methods, instructions or products referred to in the content.